Chapter 3. Structures, Growth and Condensation Mechanism of Titanate Nanostructures Produced by Hydrothermal Method

3.1. Introduction

In Chapter 2, we reported two principal sodium titanate structures obtained in the hydrothermal synthesis: lepidocrocite-type and rutile-type titanates. The various lepidocrocite-type products involve nanowire, nanotube, semi-nanotube and nanosheet; the rutile-type one is submicro-stick. Although the nanotube[1-3] and nanowire[4-6] have been synthesized and their possible structures have been reported, there is still no final conclusion about the real titanate structure and growth mechanism. The stepped titanate layer structure $Na_2Ti_3O_7$ is the mostly accepted one in the published literatures.[2,4,5] However, the lepidocrocite type layer structure seems to more reasonable due to the observations of XRD and Raman spectroscopy.[7] As for the rutile-type titanate submicro-sticks, it has never been published.

Therefore, in this chapter, we studied various titanate nanostructures by TEM, and then proposed our opinions of their possible structures. In the end of this chapter, we try to give a reasonable growth mechanism to explain our observations mentioned above and the structural doubts in published literatures.

3.2. Method

3.2.1. High-resolution TEM image (HRTEM)

The high resolution transmission electron microscopy (HR-TEM) images were

performed by Hitachi HF2000 with field emission gun electron source operated at 200 keV. The TEM samples were prepared by grinding and ultrasonic treating to disperse in ethanol solution, and then drop on holey or lacey carbon film supported on copper grid. We dried the sample at ambient in the air before transferred into TEM column chamber.

3.2.2. Electron differaction pattern (ED)

The electron diffraction pattern (ED) were carried out by Philips CM30 with LaB_6 electron source operated at 300 keV. CM30 has big tilt angle range (±60˚) in favor of studying the reciprocal lattice of our sample. The TEM samples were prepared by grinding and ultrasonic treating to disperse in ethanol solution, and then drop on holey or lacey carbon film supported on copper grid. We dried the sample at ambient in the air before transferred into TEM column chamber.

3.2.3. Simulations of TEM result

All TEM simulations were performed by specialized program “Mac Tempas” with the parameters (include cell parameter, space group, thickness and defocalization) of each unique structure predicted respectively.

3.3. Structures of the lepidocrocite type products

3.3.1. nanoribbon

For structural discussions of the lepidocrocite type products, such as nanotube, nanosheet and nanoribbon, we must start from the nanoribbon due to its better crystallized structure which can provide clearer structural information. The possible structure of nanoribbon has

been proposed as $Na_2Ti_4O_9$[8] and $Na_2Ti_3O_7$[9]. Actually, the distance of fringe repeating unit (Section 2.3 and figure 3.1b) is 10 Å, which is according to neither tetra-titanate (12 Å) nor tri-titanate (9 Å). The composition of nanoribbon characterized by EDX and TGA-MS is about $(NaOH)_{0.5}\cdot TiO_2$ excluding intercalated carbonate 0.02 CO_2 and absorbed water 0.3 H_2O. In ED pattern observations (figure 3.1a), we found that the symmetry of intensity along c axis is per 7 points and the reflection condition is h=2n as (h00), l=2n as (00l) and h+l=20 as (h0l). These observations is not according to typical stepped layer structured $Na_2Ti_4O_9$ (monoclinic, space group: C2/m) and $Na_2Ti_3O_7$ (monoclinic, space group: P2/m), although the reflection conditions is agree with C2/m symmetry but the repeating unit is 7 (not 4). In HREM, we can obviously observe that repeating symmetry unit is half of this septa-titanate, it implies that there is a mirror symmetry in the center of unit cell and perpendicular with the c axis. The XRD and Raman results (Section 3.7.1) reveal that this structure is closer to lepidocrocite type layer structure (n=∞). All the evidences reveal that the nanoribbon is not typical stepped layer structure.

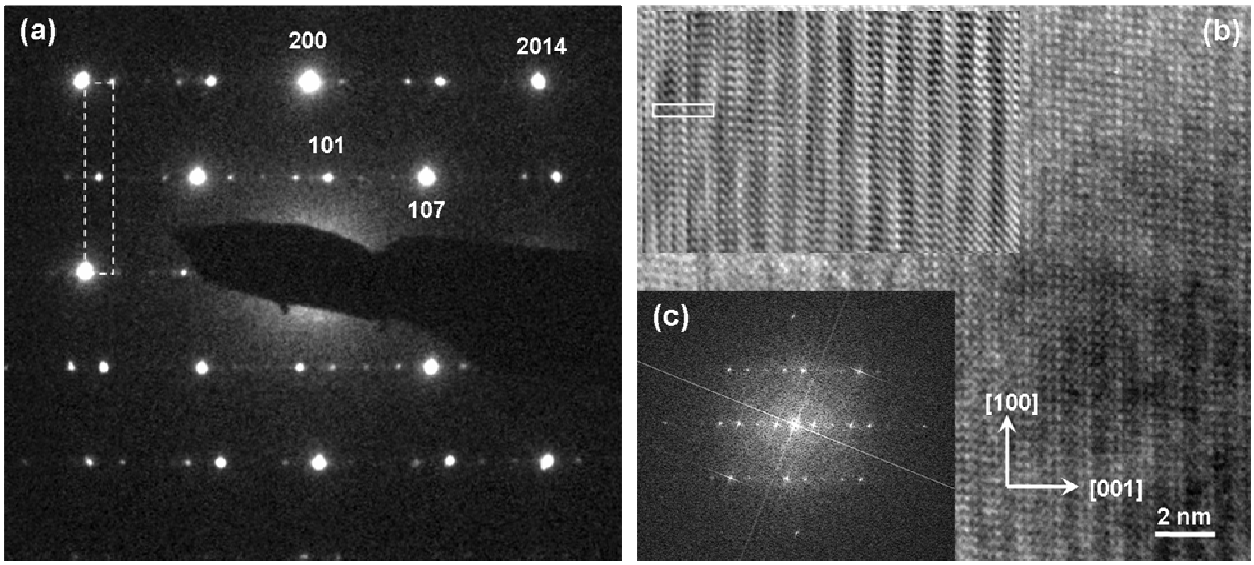

Figure 3.1. (a) SAED, (b) HRTEM and (c) FT pattern (above is inversed FT pattern) of HR image of nanoribbon (RDH10M220) viewing along [010].

Therefore, we proposed a possible structure as "$Cs_2Ti_6O_{13}$" type sodium hydroxo titanate $NaTi_2O_4(OH)$ with monoclinic system, space group I2/m and cell parameter as a = 3.65 Å, b = 17 Å, c = 20 Å, β= 87° (figure 3.2). The angle beta (only 3° difference from 90°) can be observed carefully in both ED and TEM, which implies that there is some distortion along the plane (101). We are of opinions with this distortion is from the misfit between sub-lattice distance of Ti-O (3.75Å×3.0 Å) and Na-O (3.4 Å ×3.4 Å). The "$Cs_2Ti_6O_{13}$" type sodium hydroxo titanate layer structure is constructed by stacking of two NaCl type sub-lattices along the (010) direction ($Ti_2O_3(OH)$ and NaO sub-lattice stacking layer by layer).

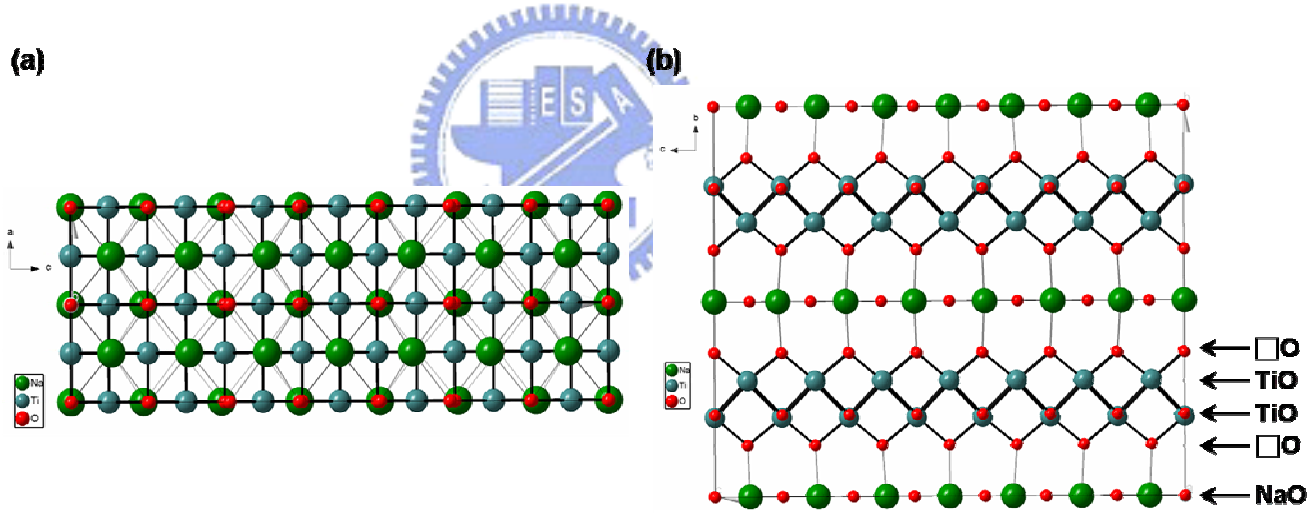

Figure 3.2. Possible structure expressed as ball and stick mode of the nanoribbon as "$Cs_2Ti_6O_{13}$" type titanate $NaTi_2O_4(OH)$ viewing along (a) [010] and (b) [100].

For further comparison of the assumed structure and TEM observations, the simulation of ED and HRTEM has been performed by Mac Tempas with a idealized structure model as monoclinic system, I2/m space group : a = 3.65 Å, b = 17 Å, c = 20 Å, β = 87°. In figure 3.4,

the simulated ED pattern is viewing along [010], its intensity and position are almost perfectly similar with the observed one in figure 3.1. For HRTEM, the observed image viewing along [010] in figure 3.4b has been found matched with simulated image of the $NaTi_2O_4(OH)$ (focal –850; Thickness 42.5 nm) in idealized structure model.

Due to the misfit of Ti-O and Na-O sub-lattice, the real position of atom in the $NaTi_2O_4(OH)$ structure is only simply completely predicted. The further thermodynamic energy calculation and XRD refinement are under studying. Moreover, the carbonate should also be considerable. The role of carbonate in the structure is under studying too.

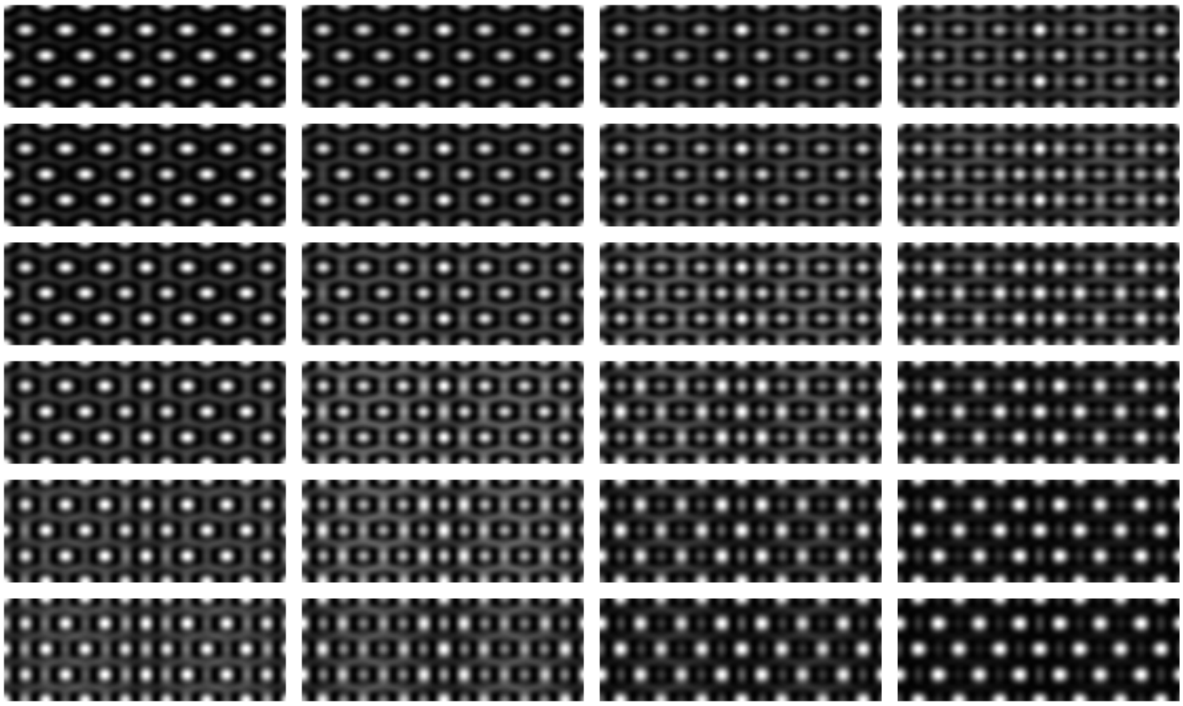

Figure 3.3. Series of HRTEM simulation of $NaTi_2O_4(OH)$ perform by Mac Tempas with I2/m space group : a = 3.65 Å, b = 17 Å, c = 20 Å, β = 87°; Focal serie: Δf (beg.-700 ; inc. 50 ; end -850) vertical ; Thickness (beg. 42.5 nm; inc. 1.7 nm; end 51 nm) horizontal.

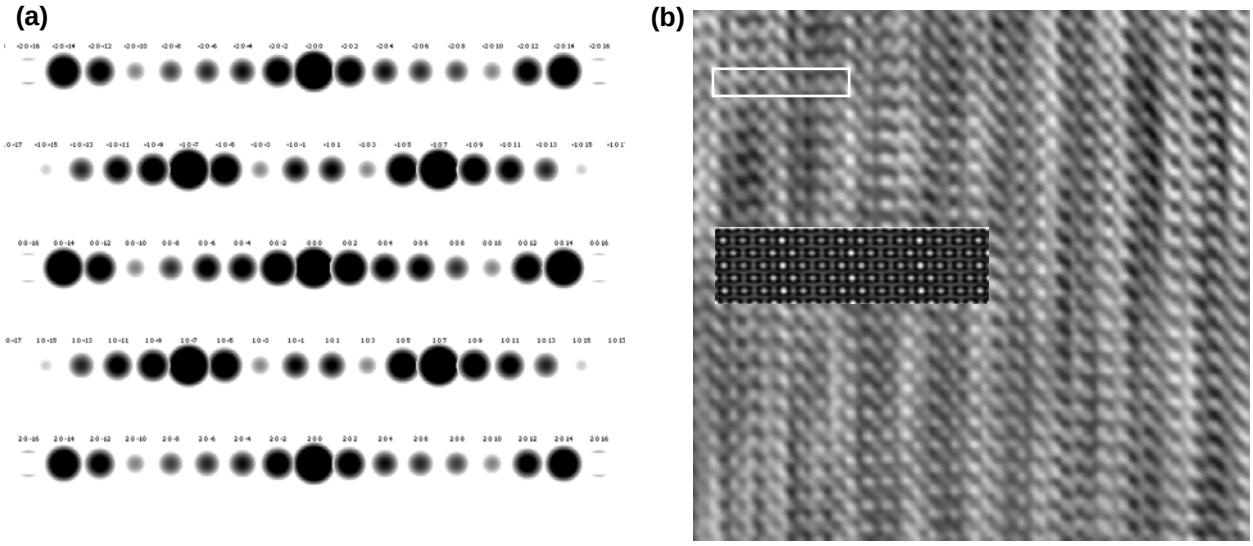

Figure 3.4. (a) ED simulation and (b) HRTEM images: observed and simulated (focal –850; Thickness 42.5 nm) from idealized structural model of "$Cs_2Ti_6O_{13}$"-type $NaTi_2O_4(OH)$ viewing along [010].

3.3.2. nanotube and nanosheet

The nanotube, nanosheet and nanoribbon have similar structure but different morphologies from different conditions. The nanoribbon is longer (a-axis direction of the $NaTi_2O_4(OH)$) and more planar (a, c plane) obtained in 10M $NaOH_{(aq)}$ at higher temperature (180˚ C) (ex. RDH10M180) or small grain sized precursor in 10M $NaOH_{(aq)}$ at the environment existing carbonate (ex. am10MR). The nanosheet is from the bigger precursor in high concentration base solution reflux (RDH15MR) or small precursor in lower basic concentration solution (am1M120). It is a little of distorted and curved, the weaker intensity of XRD peaks of 24˚, 28˚ and 48˚ (See Section 2.3) than nanotube and nanoribbon implies that it lost other symmetry besides interlayer distance due to the turbostratic structure. The nanotube is in a critical condition: big sized precursor, 10M NaOH and at 110-150˚ C. It is rolling up starting form a monolayer of titanate.

After proton-exchanging and calcinations, the nanotube and nanosheet transform directly to anatase without through the metastable phase such as TiO_2(B). This phenomenon infers that the nanotube and nanosheet are not anti-phased layer structure as "$Cs_2Ti_6O_{13}$"-type (C-centered) but phased layer structure as typical lepidocrocite (γ-FeOOH) (Primitive). These results are relative with the structure of the intercalated Na-O sub-lattice and amount of dangling OH on the Ti-O sub-lattice. We discovered the quantity of sodium is more in nanoribbon case (Na/Ti≈0.5) and less in nanotube (Na/Ti≈0.3-0.4) and nanosheet (Na/Ti≈0.3-0.5). On the other hand, the nanotube and nanosheet have more OH containing. We inferred that the layer is planar if Na is more to saturate and fix the layer structure of sub-lattice of NaO, and more curve due to OH dangling change the surface energy of TiO layer. Therefore, the lamellar product obtained in low basic concentration or high concentration. The further one is due to lower OH concentration to curve, and the latter is due to saturated Na ion intercalated. However, the precursor size and carbonate in the structure should be considered. The nanosheet is also obtained when precursor is too small and the product layer is not wide enough for rolling up. Moreover, the carbonate interlayer can stabilized the layer structure to lead to more planar structure.

3.4. Structure of the rutile type (lamellar ramsdellite) product

The rutile type submicrostick is a quite different structure from other products. Its sodium quantity containing is more (Na/Ti=0.57) and less of OH. The density measurement reveals that it is the most condensed structure than other titanate nanostructures ($d=3.22 gcm^{-3}$).

In small angle XRD result, we can observe that it has a very low angle peak at 2.2˚ (40.9Å). That implies that it has a very long axis in the unit cell. For further structural information, we rebuilt the reciprocal lattice by Philips CM30 TEM (tilt angle range= ±60˚) with a double-tilt sample holder. We tilted and record sequentially the selected area electron diffraction pattern (SAED) on a well isolated crystallite as figure 3.6 exhibited. In figure 3.6, we tilted the axis (the axis b) of submicrostick. We reconstructed the 2D reciprocal lattice of a, c plane and found lattice parameters: a=40.9Å, b=2.9Å c=9.4Å, β=80˚. Due to these lattice parameters and the reflection conditions of ED, we inferred that it is monoclinic, primitive system.

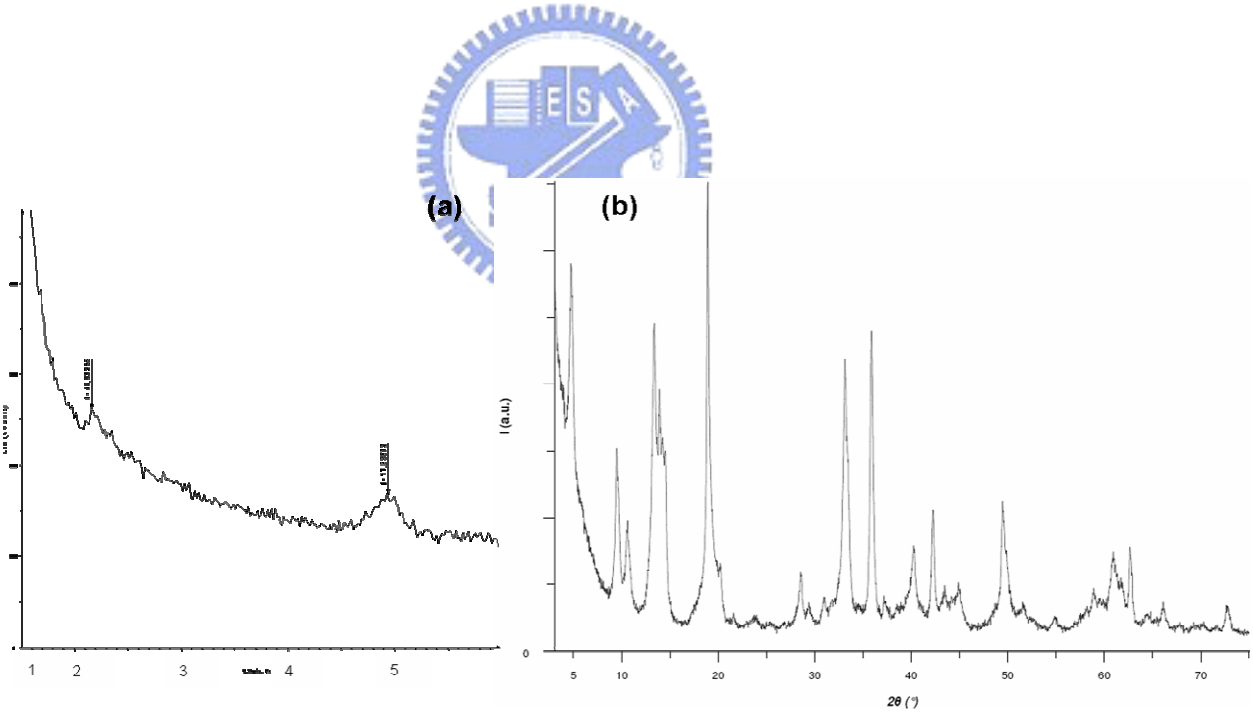

Figure 3.5. (a) Small angle XRD and (b) powder XRD diagrams of the submicrosticks (rut10M220).

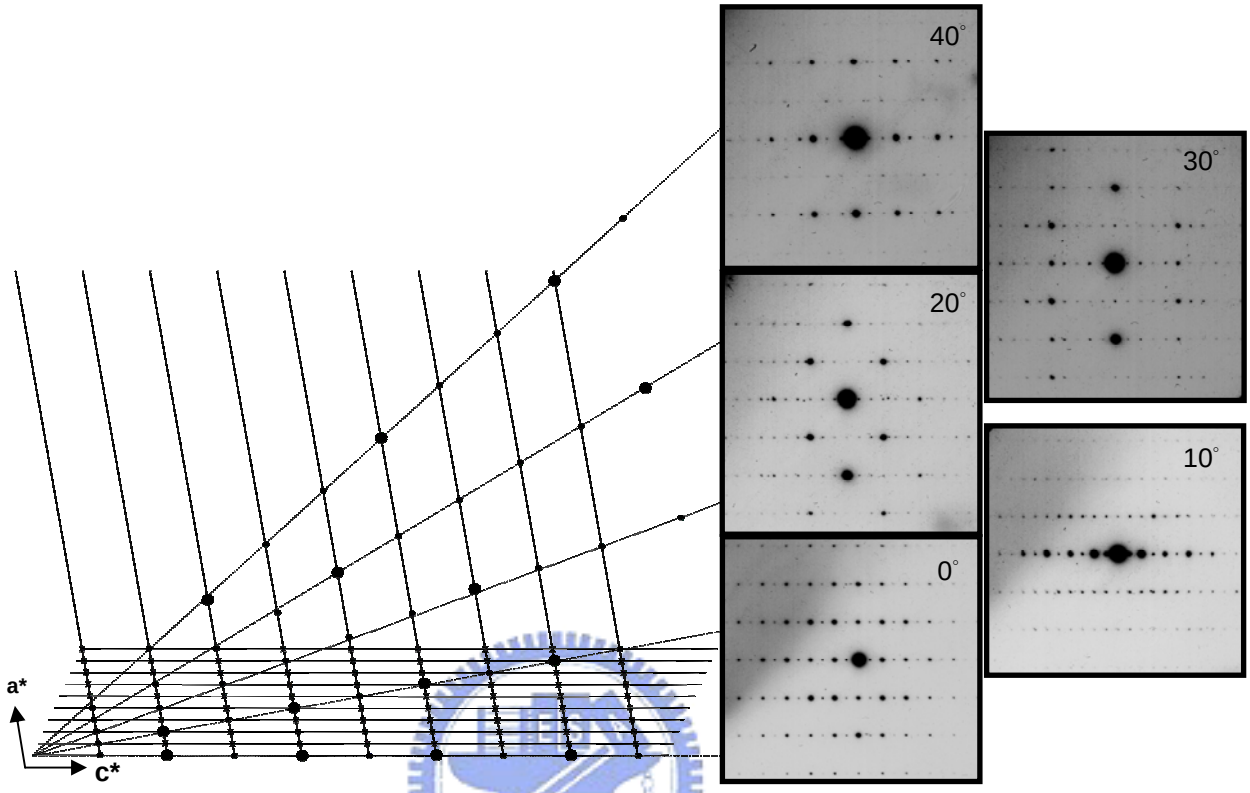

Figure 3.6. The diagram of reciprocal lattice reconstructed by tilting single crystallite along [010] of the submcrostick.

In HRTEM images along [100], we can clearly observe the distance of 4.7Å (1/2 of c) and 3Å (b). Besides, we can observe a long range misfit by the difference of contract and the regular change atomic image arrangement along [010].

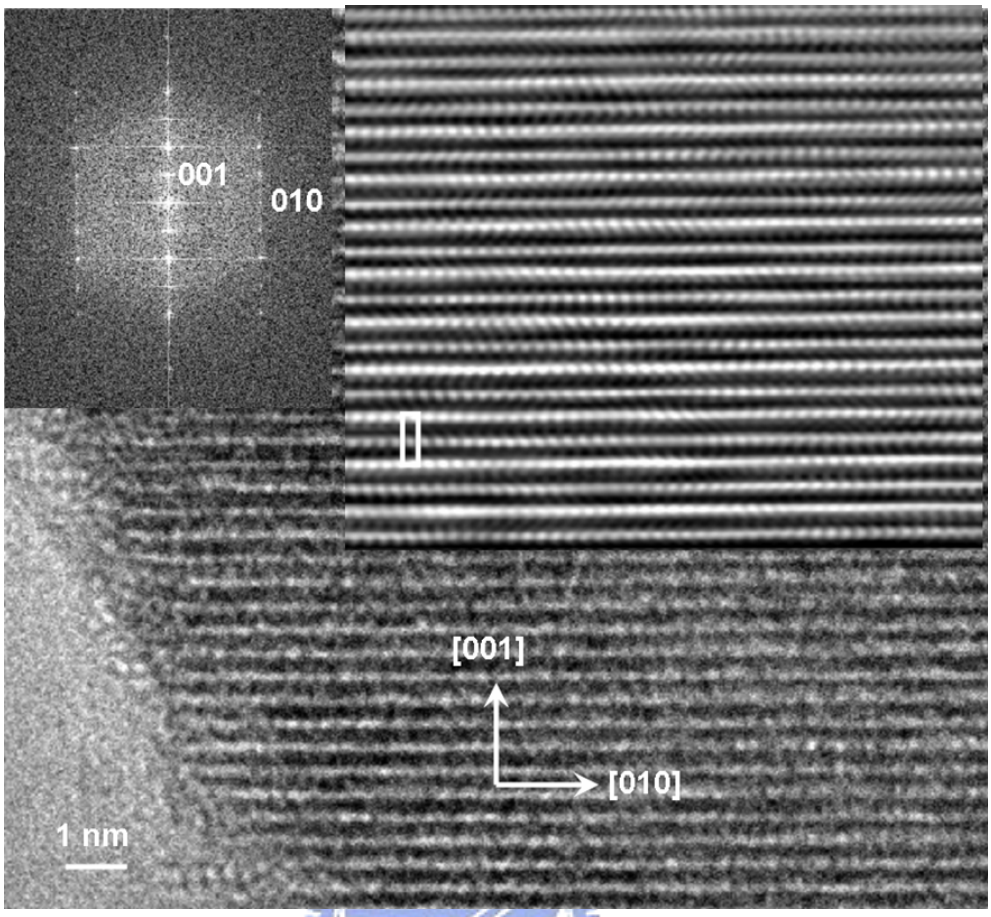

Figure 3.7. HRTEM image and the FT and inverse FT patterns of the submicrostick viewing along [100].

According to the observations above-mentioned, we inferred a possible structure and unit cell of this rutile type titanate as lamellar ramsdellte (See figure 3.8). The 4.7Å distance in HRTEM is the same with hollandite and ramsdellite. Besides, it has very long axis of unit cell possibly due to symmetry of interlayer. The excellent cation mobility (be able to completely proton exchange in ambient) is also reveals that it is lamellar or with very big sized tunnel. Therefore, we implied that it is as "lamellar ramsdellite". However, we don't know the correct atomic position in the unit cell. Such big lattice leads to hardly predict the atomic positions. Further refinement of lattice parameters is under studying. The lamellar ramsdellite can be regarded as derive of lepidocrocite. In fact, the lamellar ramsdellite is only different along c from the $Cs_2Ti_6O_{13}$ type lepidocrocite structure. Moreover, they have different preferred

orientation: the axis direction of lepidocrocite type one is a (= c of lamellar ramsdellite), and the axis direction of lamellar ramsdellite is b (= c of lepidocrocite one). The evidences of their similar structure but different preferred orientation are the similar results on Raman and XAS (See Section 3.7 Annex).

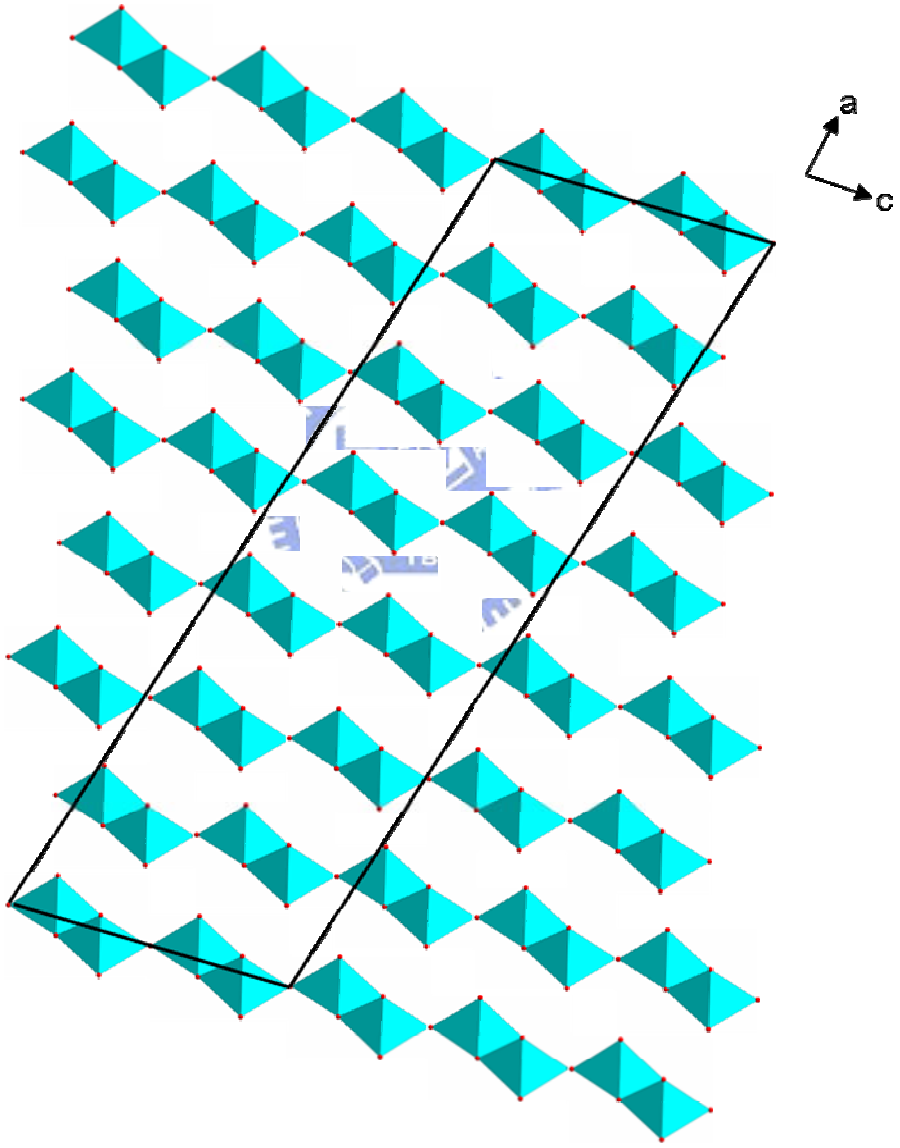

Figure 3.8. The possible structure viewing along [010] of the microstick as lamellar ramsdellite with lattice parameters: monoclinic, Primitive, a=40.9Å, b=2.9Å c=9.4Å, β=80°.

3.5. Growth mechanism and phase transformations of the sodium hydroxo titanates

For explaining all the observation mentioned above, we proposed the possible growth mechanism of lepidocrocite type and lamellar ramsdellite titanate nanostructure starting from titanium dioxide with different structures (anatase, brookite and rutile), respectively.

In the transformation from anatase to lepidocrocite (figure 3.9), the bulk anatase will dissolve in the concentrated NaOH aqueous solution to form the zigzag chain unit by dividing along (010) plane. This zigzag chain is equal to zigzag chain unit along [101] direction of lepidocrocite type titante structure. Therefore, they can recombinate as lepidocrocite monolayer by oxolation in basic solution.

In the case of brookite (figure 3.10), it forms also the same zigzag chain unit with anatase dividing along (010) plane. In fact, the zigzag chain is the main building block of polycondensation to brookite. Although we have not employed the brookite as precursor, we can observe similar results in the literature published by Meng et al.[10] They proposed that brookite and anatase can both transform to the nanoribbon, which is a powerful evidence to prove our predictions. Another evidence is we can observe the brookite become more in more basic environment (compare am0M120 and am0.1M120).

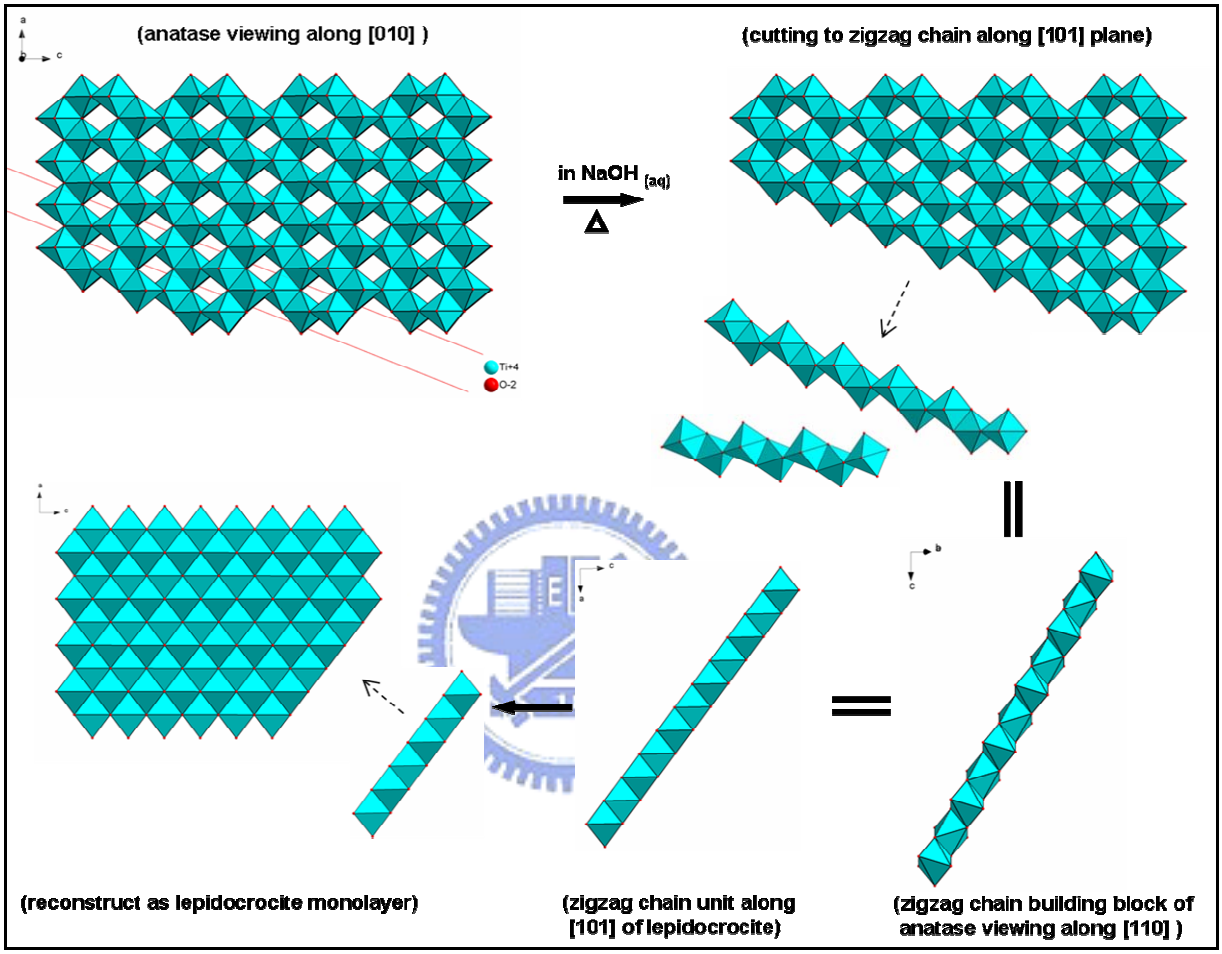

Figure 3.9. Possible growth mechanism from anatase to lepidocrocite.

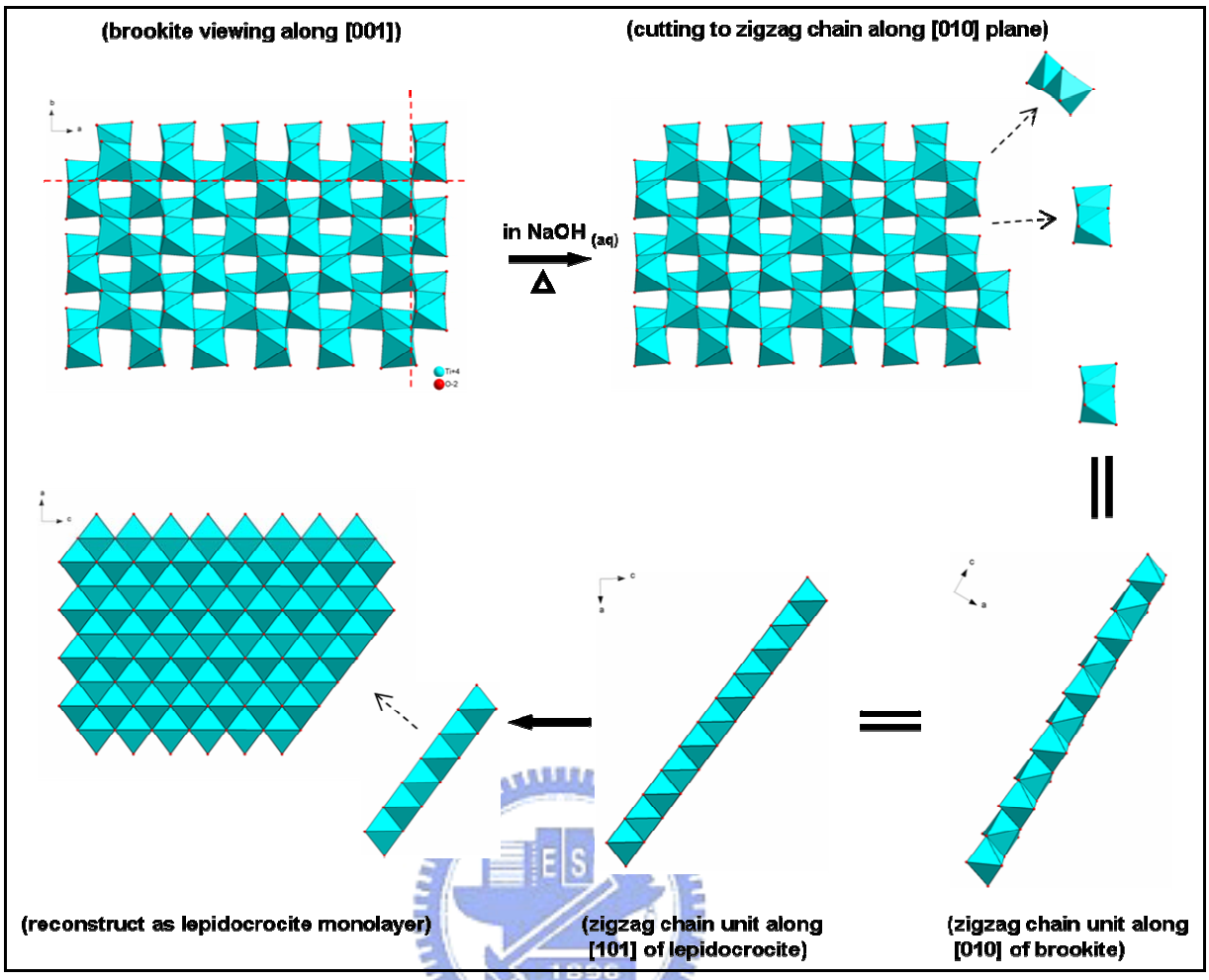

Figure 3.10. Possible growth mechanism from brookite to lepidocrocite.

The rutile forms the different chain unit (figure 3.11) from anatase and brookite in concentrated basic solution. This chain is divided along [001] and linear form (not zigzag). It can be reconstructed to lepidocrocite layer along [100] direction in lower temperature.

In higer temperature, it is another story (figure 3.12), the rutile linear chain building block can reconstruct to lamellar ramsdellite directly. Therefore, we can observe the lamellar ramsdellite product from rutile precursor even in 180˚ C.

The anatase and brookite chain possibly further deconstructs in high temperature to smaller unit as building block as ramsdellite type double chain unit or rutile type linear chain, and then transform to lamellar ramsdellite. The bigger sized precursor is not easy to further deconstructions due to its longer chain unite. According to this reason, RDH is still

lepidocrocite as major in 220˚ C.

The amorphous is not crystallized; therefore its building block form depends upon the environment, such as temperature and basic concentration. That is why it forms lamellar ramsdellite at 220˚ C and lepidocrocite at lower temperature.

The growth mechanisms we proposed can well explain all the observation above mentioned. The bigger initiator form larger crystallite due to the longer chain like building block. The different structure precursors exhibit different transformations due to formation of different building block. The morphology of building block depend upon the nature of precursor, basic concentration and temperature.

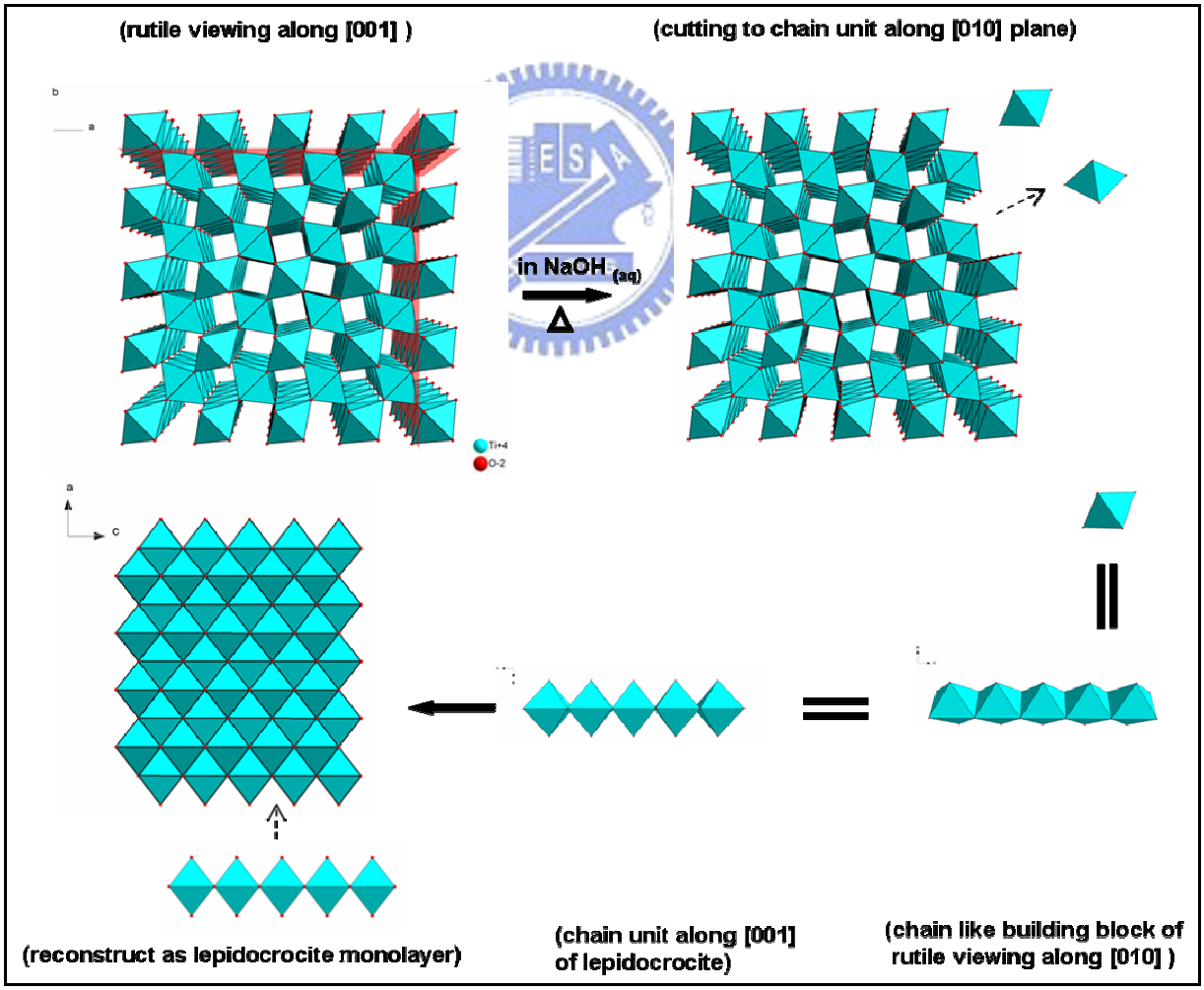

Figure 3.11. Possible growth mechanism from rutile to lepidocrocite.

The building blocks only govern the layer structure and the size. The curvature and morphology is governed by the structure of NaOH sub-lattice, and carbonate species in the structure.

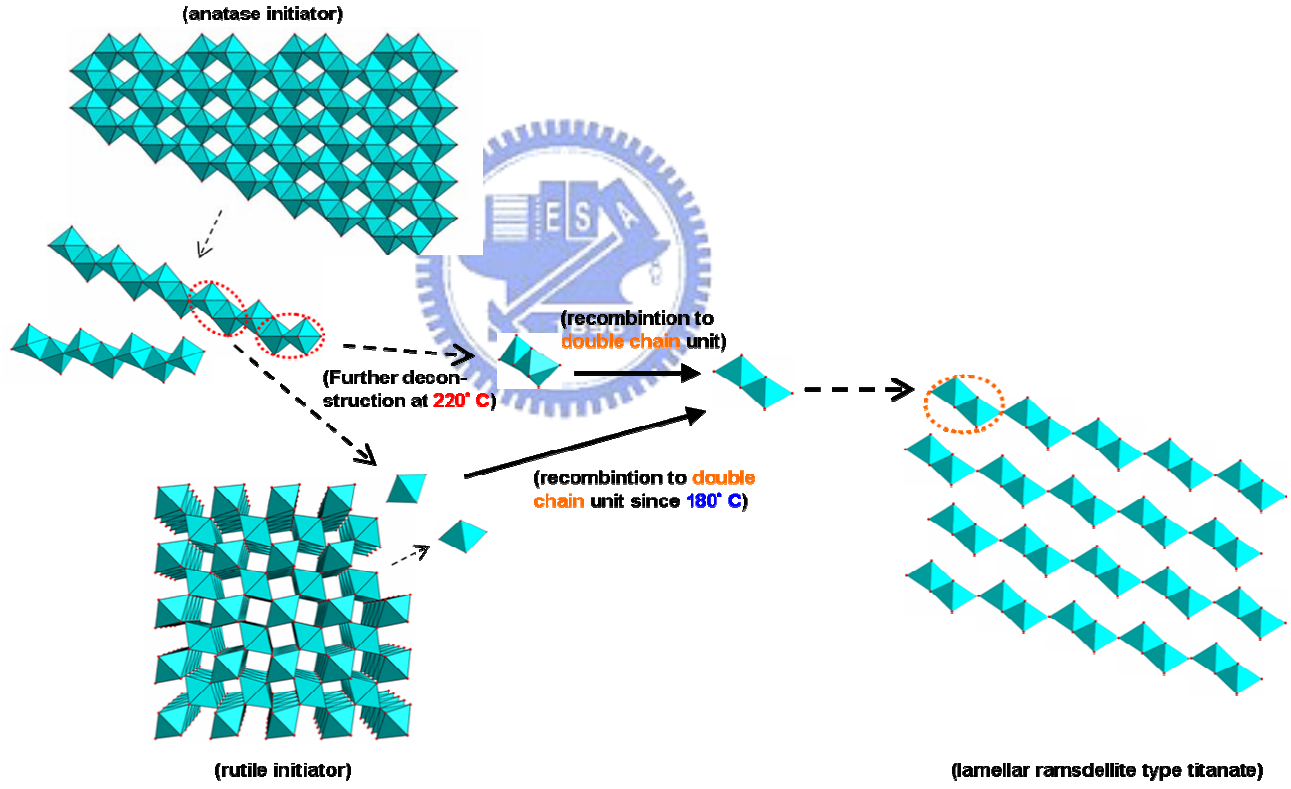

Figure 3.12. Possible growth mechanism of lamellar ramsdellite type titanate.

3.6. Conclusions

The nanoribbon structure is "$Cs_2Ti_6O_{13}$" lepidocrocite type titanate with stacking of sub-lattice NaO and TiO (layer by layer) along [010]. Its lattice parameters is monoclinic system, I2/m space group : a = 3.65 Å, b = 17 Å, c = 20 Å, β = 87°. The cell distance misfit between NaO and TiO sub-lattice cause the observation of a series fringe (repeating unit) distance 10Å between stepped layerd tritanate (9Å) and tetratitante (12Å) in HRTEM. The nanotube and nanosheet have similar structure with nanoribbon but primitive symmetry (phased layers along interlayerd axis direction) with less amount of sodium and more hydroxyl groups which cause more curved structure. The submicrosticks obtained at 220° C from small crystalline and rutile phase precursor is rutile derive new layer structure as lamellar ramsdellite with lattice parameters: monoclinic, Primitive, a=40.9Å, b=2.9Å c=9.4Å, β=80°.

The final product structure depends on the nature of initiator and the intermediate from it. In low temperature condition, the anatase and brookite phase precursor can form zigzag chain building block and then reconstruct to lepidocrocite type layer structure. The rutile one may deconstruct to chain liked unit and form also lepidocrocite in lower temperature condition (<180° C). However, we can observe lamellar ramsdellite phase at medium temperature as 180° C. The linear chain unit may directly construct to double chain building block of ramsdellite when temperature >180° C. The anatase initiator is not easy to transform to lamellar ramsdellite type titanate, beside of high temperature as 220° C and small crystalline initiator such as amorphous and P25, because of their zigzag chain intermediate can further deconstruct to small species such as single TiO_6 octahedron (building block of linear single chain of rutile) or two octahedrons sharing by edge (building block of double chain of ramsdellite). These small clusters may reconstruct as lamellar ramsdellite type structure in high temperature.

3.7. Annex

3.7.1. Raman study

We employed FT-Raman for further structural information study. Unfortunately, there are not many reports about the Raman discussions of titanate, and the exact assignment of the Raman spectra is still not available. We can only compare our results with other groups to discuss possible tendency.

In figure A3.1, we compared different products obtained such as nanosheet, nanotube, nanowire and submicrostick. We discovered their principal band positions are almost the same, only different intensity and sharpness of peaks. This implies that they have similar titanate layer structure. For example, titanate nanotube has broad bands at 86 cm^{-1}, 129 cm^{-1}, 163 cm^{-1}, 193 cm^{-1}, 277 cm^{-1}, 386 cm^{-1}, 448 cm^{-1}, 558 cm^{-1}, 662 cm^{-1}, 702 cm^{-1}, 800 cm^{-1} and 910 cm^{-1}; the nanowire has sharper peaks at 86 cm^{-1}, 108 cm^{-1}, 166 cm^{-1}, 196 cm^{-1}, 239 cm^{-1}, 279 cm^{-1}, 311 cm^{-1}, 373 cm^{-1}, 428 cm^{-1}, 473 cm^{-1}, 598 cm^{-1}, 672 cm^{-1}, 704 cm^{-1}, 771 cm^{-1}, 882 cm^{-1} and 920 cm^{-1}.

The published reports concluded that 290 cm^{-1} and 660 cm^{-1}-760 cm^{-1} are due to Na-O-Ti as Na_2O-TiO_2 glass.[7,8] The 440 cm^{-1} and 600 cm^{-1} are Ti-O bending and stretching vibration involving six-coordinated Ti and three-coordinated O.[9] The 850 cm^{-1}-950 cm^{-1} is stretching modes of Ti-O stick out into the interlayer space.[10] We compare Raman spectra of the nanotube and various bulk solid state synthetic titanates (figure A3.2). We found the Raman spectrum of nanotube is very similar as lepidocrocite type cesium titanate and all results agree well with the mentioned rule. The 910 peak is weak in our samples, lepidocrocite and tunnel structure titanates without Ti-O stick out into the interlayer space. On the other hand, $K_2Ti_2O_5$, $K_2Ti_4O_9$ and $Na_2Ti_3O_7$, which are stepped layer titanate, have strong peak near 900 cm^{-1}. That implies our product may be lepidocrocite type structure.

We also found a weak band appears at 1060 cm^{-1} when carbonate existed (figure 3.3, orange arrow marked). That provides another way to observe carbonate existed.

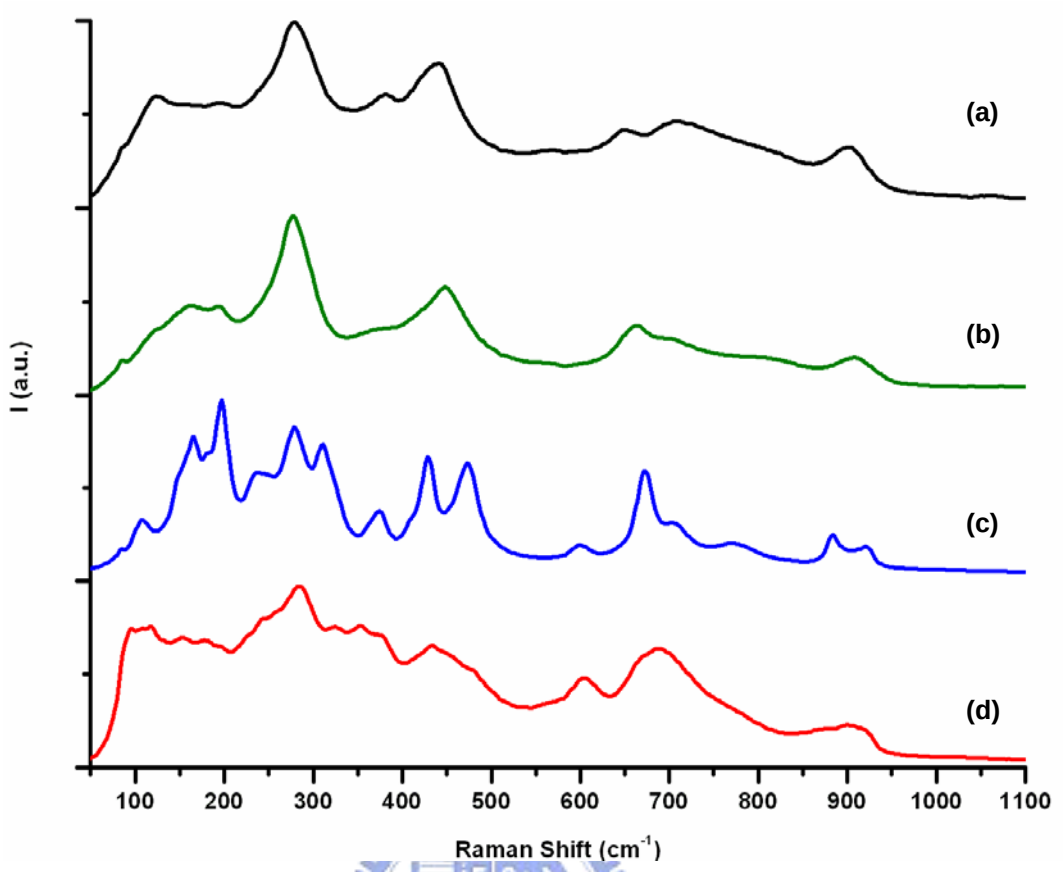

Figure A3.1. Raman spectra of (a) nanosheets (am1M120), (b) nanotubes (RDH10M140), (c) nanowires (RDH10M180) and (d) submicro-sticks (rut10M220).

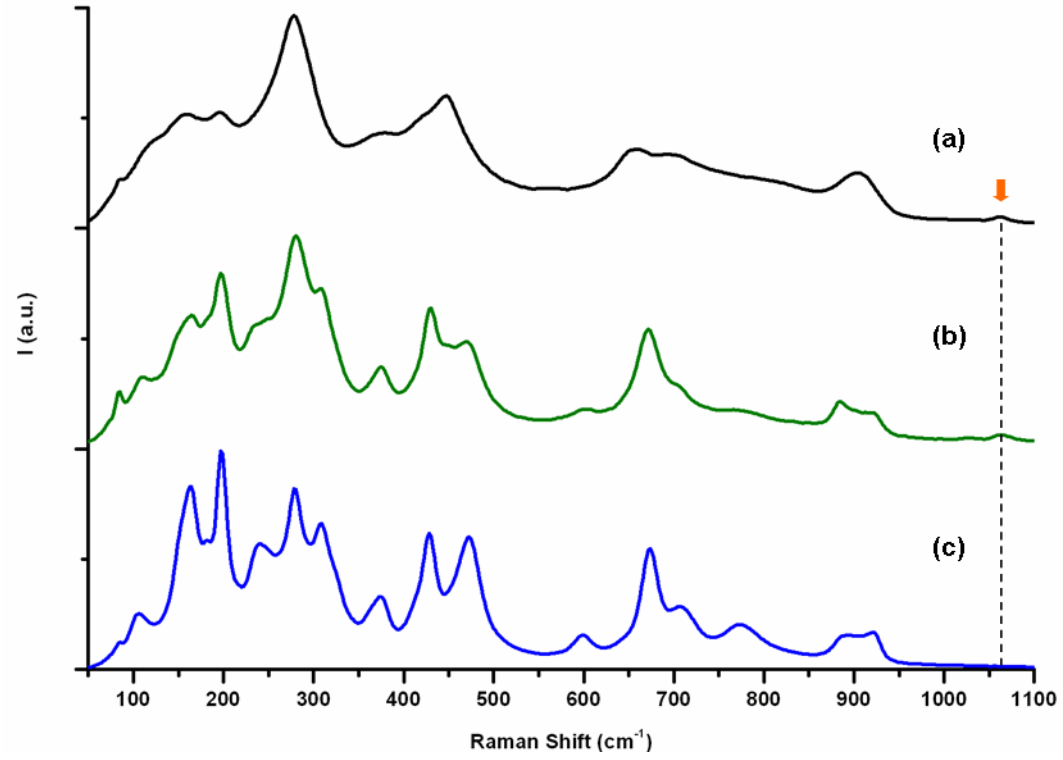

Figure A3.2. Raman spectra of (a) RDH5M120-0.8CO3, (b) am10MR, (c) am10M180.

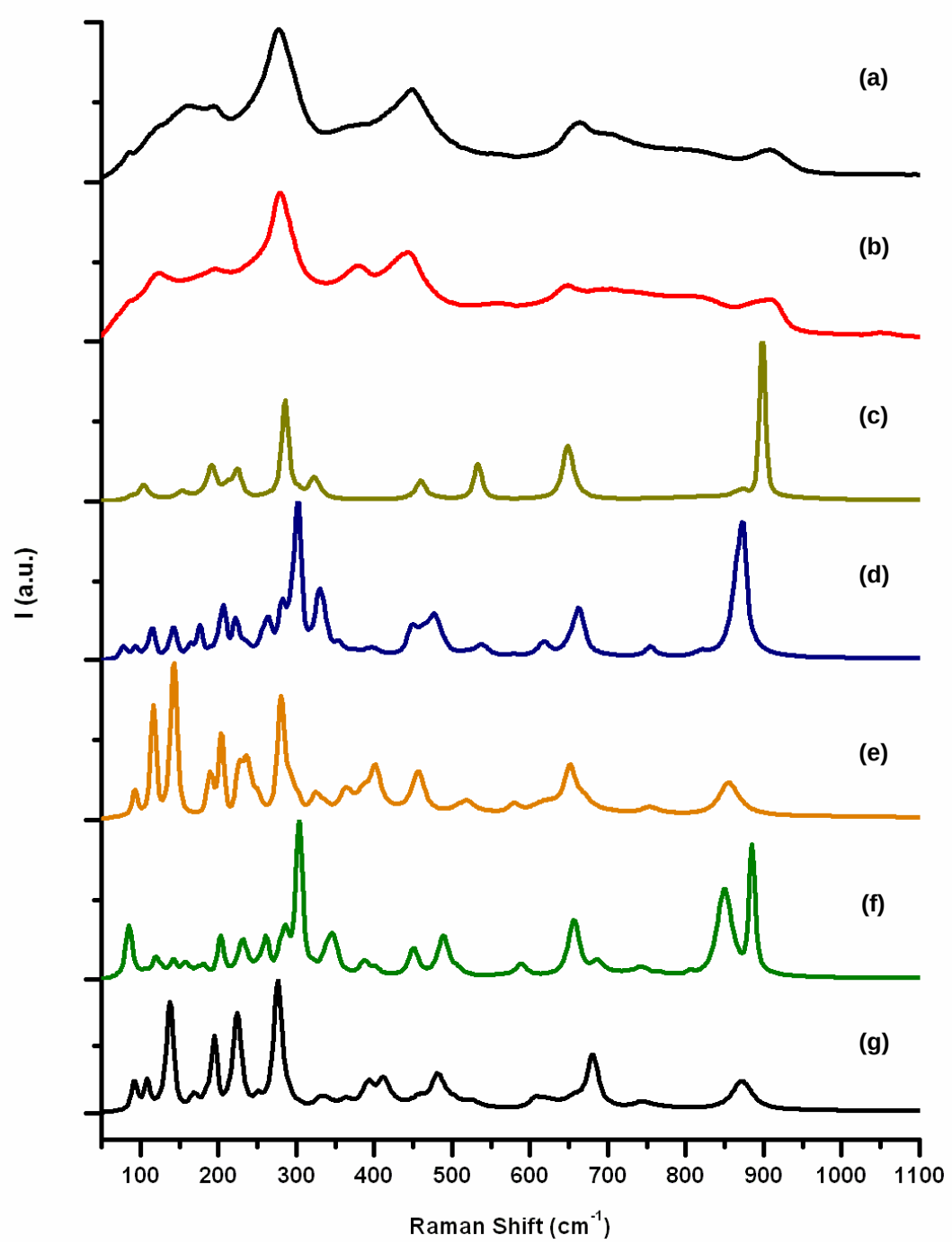

Figure A3.3. Raman spectra of (a) nanotubes (RDH10M140), (b) lepidocrocite $Cs_2Ti_6O_{13}$, (c) $K_2Ti_2O_5$, (d) $K_2Ti_4O_9$, (e) $K_2Ti_6O_{13}$, (f) $Na_2Ti_3O_7$ and (g) $Na_2Ti_6O_{13}$.

3.7.2. X-ray absorption spectroscopy (XAS) study on X-ray Absorption Near-Edge Structure (XANES)

The results of X-ray absorption spectroscopy were performed by synchrotron radiation source in ESRF, Grenoble, France. We studied the K edge of titanium (~5 keV) on X-ray adsorption. The observation range is from 4750 eV to 5820 eV, 2s par point, 5eV of step size until 4937.8 eV then decrease step until 4958.7 eV, then 0.2 eV par step until 4975.4 eV, finally at k constant until the end, all operations terminated with 3eV after the edge.

According to the XANES observations, we found the submicrostick and nanoribbon exhibit similar result. That implies they have similar electron structure and chemical environment of titanium atoms. This result can indirectly prove they have similar structure of Ti-O sub-lattice in a small range. The spectrum of sample after proton-exchanging is different from the raw product. For further structural discussions, the results of Extended X-ray Absorption Fine Structure (EXAFS) are under studying.

Table A3.1. Table of XANES results of submicrostick and nanoribbon samples.

Pics	rut10M220	RDH10M180	RDH10M180-H
A1	4968.9	4968.9	4968.9
	12%	13%	13%
A2	4971.0	4970.9	4970.7
	58%	58%	50%
A3	4972.0	4972.4	4972.2
	13%	12%	20%
B	4974.0	4973.9	4973.9
	17%	17%	17%

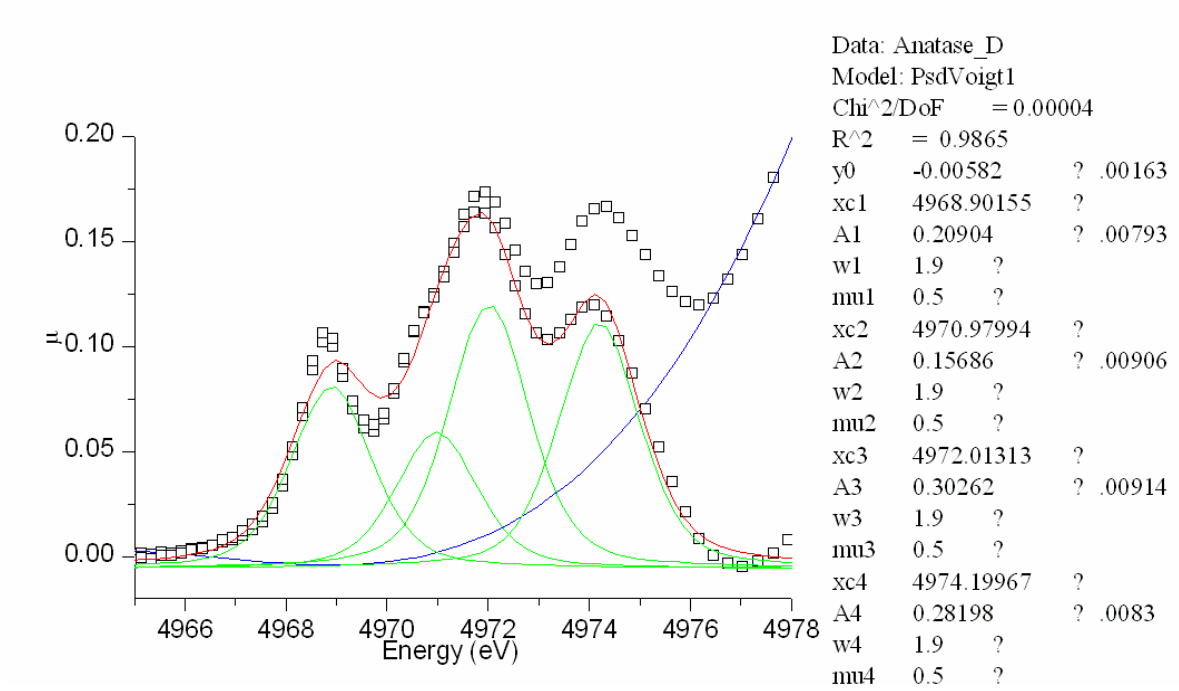

Figure A3.4. XANES of anatase TiO_2.

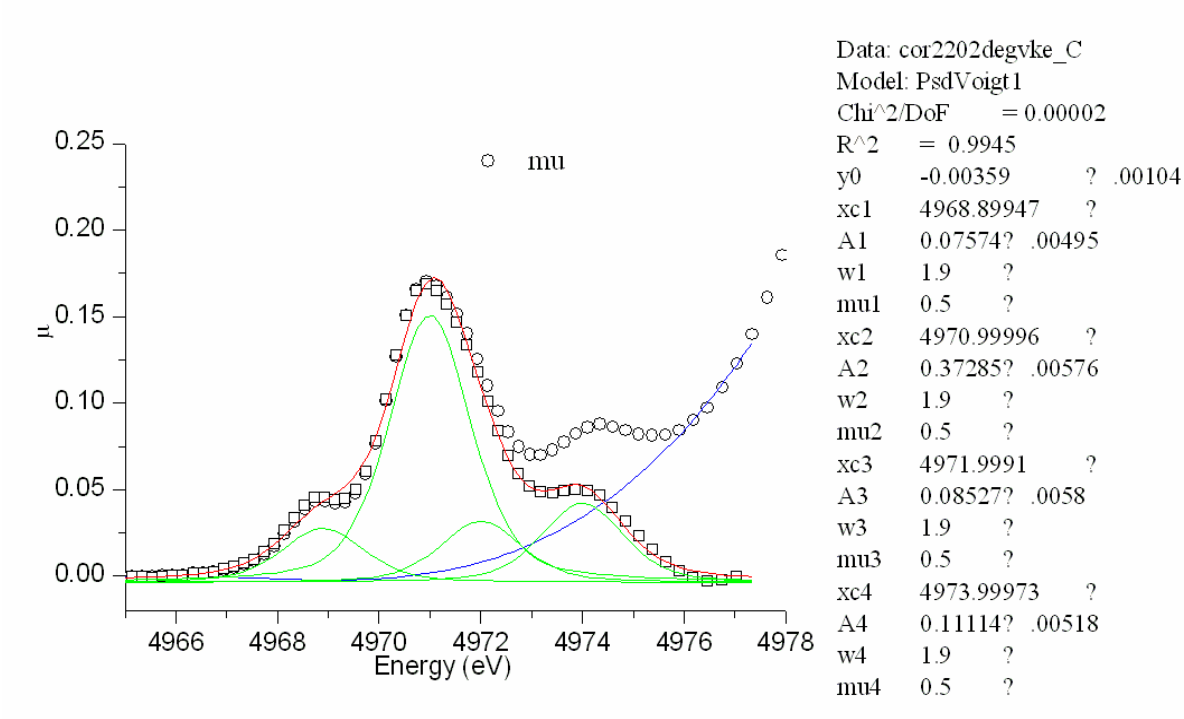

Figure A3.5. XANES of titanate submicrostick (rut10M220).

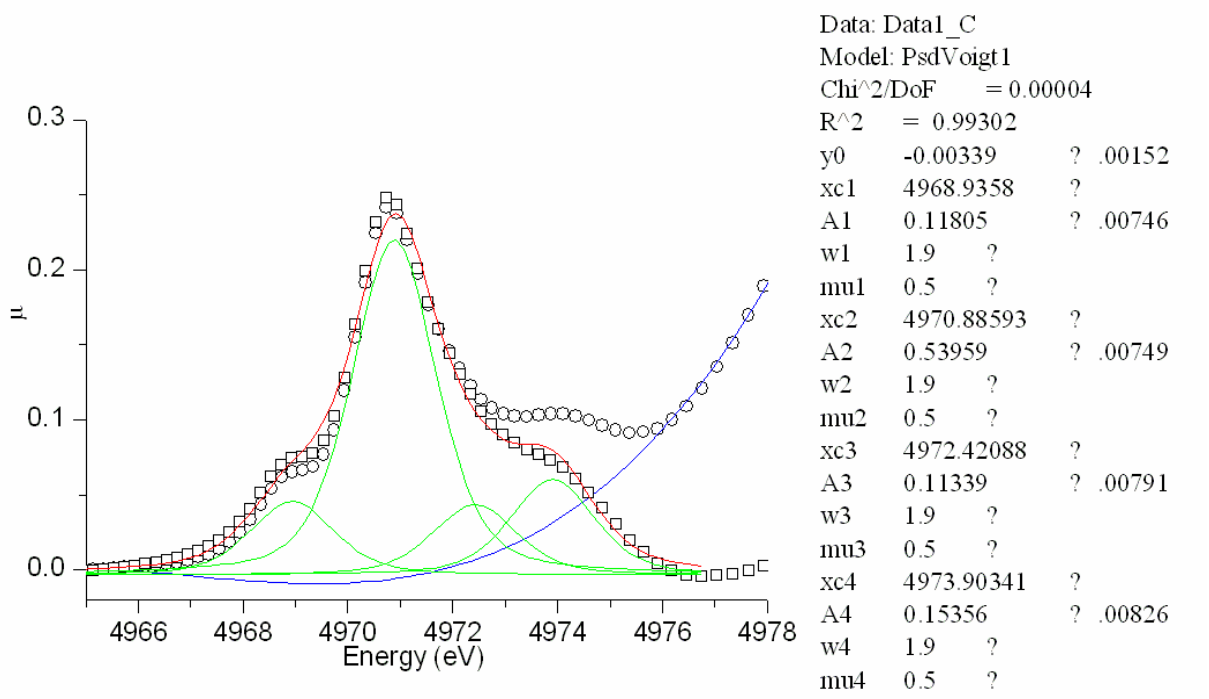

Figure A3.6. XANES of titanate nanoribbon (RDH10M180).

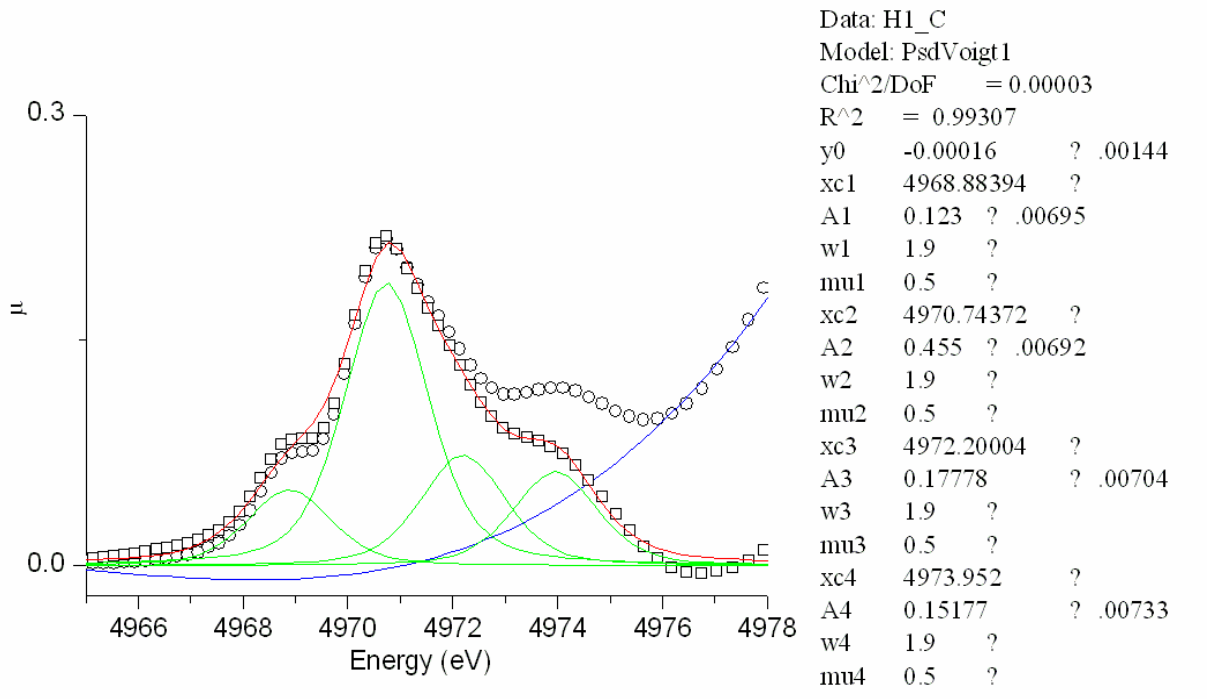

Figure A3.7. XANES of proton-exchanged titanate nanoribbon (RDH10M180-H).

3.8. Reference

[1] T. Kasuga, M. Hiramatsu, A. Hoson, T. Sekino and K. Niihara *Adv. Mater.* **1999**, 11, 1307-1311.

[2] Q. Chen, W. Zhou, G. H. Du and L. M. Peng, *Adv. Mater.* **2002**, *14*, 1208-1211.

[3] R. Ma, Y. Bando and T. Sasaki, *Chem. Phys. Lett.* **2003**, *380*, 577–582.

[4] Z. Y. Yuan, J. F. Colomer and B. L. Su, *Chem. Phys. Lett.* **2002**, *363*, 362–366.

[5] H. Zhu, X. Gao, Y. Lan, D. Song, Y. Xi and J. Zhao, *J. Am. Chem. Soc.* **2004**, *126*, 8380-8381.

[6] D. Wu, J.Liu, X. Zhao, A. Li, Y. Chen, and N. Ming, *Chem. Mater.* **2006**, *18*, 547-553.

[7] R. Ma, K. Fukuda, T. Sasaki, M. Osada and Y. Bando, *J. Phys. Chem. B* **2005,** *109,* 6210-6214.

[8] H. Zhu, X. Gao, Y. Lan, D. Song, Y. Xi and J. Zhao, *J. Am. Chem. Soc.* **2004**, 126, 8380-8381.

[9] D. Wu, J. Liu, X. Zhao, A. Li, Y. Chen, and N. Ming, *Chem. Mater.* **2006,** *18,* 547-553.

[10] X. Meng, D. Wang, J. Liu and S. Zhang, *Materials Research Bulletin* **2004**, *39*, 2163–2170.